Int. J. Therm. Sci. (2000) 39, 871–885

S1290-0729(00)01193-5/FLA

Numerical prediction of heat transfer in fluidized beds by a kinetic theory of granular flows

Achim Schmidt *, Ulrich Renz

Lehrstuhl für Wärmeübertragung und Klimatechnik der RWTH-Aachen, Eilfschornsteinstrasse 18, D-52056 Aachen, Germany

(Received 20 June 2000, accepted 27 July 2000)

Abstract — In dense gas–solid two-phase flows of bubbling fluidized beds the particle-to-particle interactions cannot be neglected and an Eulerian approach has been used to predict the fluid dynamics as well as the heat transfer. The physical properties of the solid phase can be modeled with the kinetic theory of granular medias and the governing equations are solved numerically. The present work compares different physical models for the thermal transport coefficients of the solid phase for a lab-scaled two-dimensional fluidized bed filled with mono-disperse glass beads. The numerical results show a strong correlation between fluid dynamics and the instantaneous heat transfer similar to the so-called packet theory by Mickley and Fairbanks [1]. © 2000 Éditions scientifiques et médicales Elsevier SAS

fluidization / granular materials / heat transfer / multiphase flow / granular temperature / simulation

Nomenclature

B	defined in equation (15)	
c_p	specific heat	$J\cdot kg^{-1}\cdot K^{-1}$
d_s	particle diameter	m
d_{Tube}	diameter of the heat transfer tube	m
$\boldsymbol{g}$	gravitational constant	$m\cdot s^{-2}$
g_0	radial distribution function	
h	specific enthalpy	$J\cdot kg^{-1}$
h	height	m
$\boldsymbol{I}$	identity tensor	
k_Θ	solids fluctuating energy diffusion coefficient	$Pa\cdot s$
Nu	Nusselt number	
p	pressure	$N\cdot m^{-2}$
p_s	solid pressure	$N\cdot m^{-2}$
$\boldsymbol{q}$	heat flux	W
$\dot{Q}$	heat flux	W
r	radial coordinate	m
Re	Reynolds number	
T	temperature	K
t	time	s
tr	trace of a tensor (sum of main-diagonal elements)	
$\boldsymbol{v}$	velocity vector	$m\cdot s^{-1}$
w	width	m
x	x-coordinate	m
y	y-coordinate	m

Greek symbols

α	volumetric interphase heat-transfer coefficient	$W\cdot m^{-3}\cdot K^{-1}$
α_{gs}	fluid–particle heat-transfer coefficient	$W\cdot m^{-2}\cdot K^{-1}$
α_T	heat-transfer coefficient at tube surface	$W\cdot m^{-2}\cdot K^{-1}$
β	interphase drag coefficient	$kg\cdot m^{-3}\cdot s^{-1}$
γ_Θ	dissipation of fluctuating energy	$Pa\cdot s^{-1}$
ε	volume fraction	
γ	angle	deg
κ	thermal conductivity	$W\cdot m^{-1}\cdot K^{-1}$
κ_{cyl}	defined in equation (13)	
Φ_Θ	fluctuating energy exchange	$Pa\cdot s^{-1}$
ρ	density	$kg\cdot m^{-3}$
Θ	granular temperature	$m^2\cdot s^{-2}$
τ	viscous stress tensor	$N\cdot m^{-2}$
ω	defined in equation (14)	

Subscripts

0	jet
Bulk	bulk properties
g	gas-phase
gas	gas

* Correspondence and reprints.
schmidt@wuek.rwth-aachen.de

i	$i =$ g, s (gas or solid)
m	mixture
mf	minimum fluidization
pen	penetration theory
pm	particle material
s	solid-phase
T	tube
Tube	tube
T	total
total	total
W	wall

Superscripts

$*$	parameter multiplied by the volume fraction of its phase

1. INTRODUCTION

The heat transfer in fluidized beds has been part of many investigations in the past and numerous empirical equations to calculate the heat transfer coefficients between a fluidized bed and immersed tubes have been published (Mickley and Fairbanks [1] and Gelperin and Einstein [2]): Mickley and Fairbanks assume that discrete packets of particles periodically get in contact with a heat transfer wall. This renewal of particles leads to a time-dependent heat transfer characteristic which presumes the knowledge of the duration of such a particle–wall contact time. Unfortunately, the estimation of this so-called time-of-contact is difficult and depends on the geometrical arrangement of the heat transfer areas. Besides the theoretical work, experiments were carried out (Sundaresan and Clark [3]) to analyse the mechanisms of heat transfer. With the increase of computational power the numerical simulation becomes an additional tool to predict the fluid dynamics and the heat transfer mechanisms in multiphase flows. In the recent years the fluid dynamics of a bubbling fluidized bed has been calculated with an Eulerian approach (Kuipers et al. [4] and Boemer et al. [5]). Their numerical set-up consists of a two-dimensional isothermal fluidized bed filled with glass beads. Based on the conservation equations for both phases it is possible to predict instantaneous particle volume fractions, velocity distributions as well as the pressure field. With the implementation of the energy equations of both phases the relevant heat transfer coefficients can now be calculated. Schmidt and Renz [6] calculated the heat transfer in a lab scaled fluidized bed. The correlation between instantaneous local flow conditions and time-dependent local heat transfer coefficient has been analysed by generating a single bubble rising in a fluidized bed at state of minimum fluidization. It has been shown that the local heat transfer coefficients can be predicted without additional assumptions (e.g., the contact time). This is one of the advantages over the empirical approaches. But it has to be investigated whether the physical properties in the Eulerian equations need further empirical models or if they can be replaced by approaches from the kinetic theory of granular flows.

2. GOVERNING EQUATIONS

Due to the high particle concentrations in gas–solid fluidized beds the particle interactions cannot be neglected. In fact, the solid phase has similar properties as a continuous fluid. Therefore, the Eulerian approach is an efficient method for the numerical simulation of fluidized beds. By using the kinetic theory of granular flows (Savage and Jeffrey [7] and Lun et al. [8]) the viscous forces and the solid pressure of the particle phase can be described as a function of the so-called granular temperature. In principle, the kinetic theory of granular flows has been derived from the kinetic theory of gases: while the thermodynamic temperature is a quantum of the fluctuating energy of the molecules on the microscopic scale, the granular temperature expresses the macroscopic kinetic energy of the random particle motion. This leads to the following differential equations given in Eulerian notation.

2.1. Mass balances

So far no chemical reactions are implemented, so the accumulation of mass in each phase is balanced by convective mass fluxes.

- Gas phase:

$$\frac{\partial}{\partial t}(\varepsilon_{\mathrm{g}}\rho_{\mathrm{g}}) + \nabla \cdot (\varepsilon_{\mathrm{g}}\rho_{\mathrm{g}}\boldsymbol{v}_{\mathrm{g}}) = 0 \tag{1}$$

- Solid phase:

$$\frac{\partial}{\partial t}(\varepsilon_{\mathrm{s}}\rho_{\mathrm{s}}) + \nabla \cdot (\varepsilon_{\mathrm{s}}\rho_{\mathrm{s}}\boldsymbol{v}_{\mathrm{s}}) = 0 \tag{2}$$

Each computational cell is shared by the interpenetrating phases, so that the sum over all volume fractions is unity.

2.2. Momentum balances

According to Newton's second law the change of momentum equalizes the net force on a domain. In gas–solid fluidized beds the net force consists of the viscous force τ_i, the body force $\varepsilon_i \rho_i \boldsymbol{g}$, the solid pressure force ∇p_s^*, the static pressure force $\varepsilon_i \nabla p$ and the interphase force $\beta(\boldsymbol{v}_i - \boldsymbol{v}_j)$ which couples the gas and solid momentum equations by drag forces.

- Gas phase:

$$\frac{\partial}{\partial t}(\varepsilon_g \rho_g \boldsymbol{v}_g) + \nabla \cdot (\varepsilon_g \rho_g \boldsymbol{v}_g \boldsymbol{v}_g) = \nabla \cdot \tau_g - \varepsilon_g \nabla p + \varepsilon_g \rho_g \boldsymbol{g} - \beta(\boldsymbol{v}_g - \boldsymbol{v}_s) \quad (3)$$

- Solid phase:

$$\frac{\partial}{\partial t}(\varepsilon_s \rho_s \boldsymbol{v}_s) + \nabla \cdot (\varepsilon_s \rho_s \boldsymbol{v}_s \boldsymbol{v}_s) = \nabla \cdot \tau_s - \nabla p_s^* - \varepsilon_s \nabla p + \varepsilon_s \rho_s \boldsymbol{g} - \beta(\boldsymbol{v}_s - \boldsymbol{v}_g) \quad (4)$$

In this paper the drag function of Syamlal et al. [9] is used. The solid phase properties (i.e. solid pressure and solid viscosity) can be described with the help of the kinetic theory of granular flows. A more detailed discussion is given in Boemer et al. [5].

2.3. Energy balances

The energy equations have to take into account the thermal conduction within the phase, the heat exchange between gas and solid phase, the viscous dissipation and the term involving the work of expansion of the void fraction.

- Gas phase:

$$\frac{\partial}{\partial t}(\varepsilon_g \rho_g h_g) + \nabla \cdot (\varepsilon_g \rho_g h_g \boldsymbol{v}_g) = -\nabla \cdot \varepsilon_g \cdot \boldsymbol{q}_g + \alpha(T_s - T_g) + \tau_g \cdot \nabla \cdot \boldsymbol{v}_g + \varepsilon_g \left[\frac{\partial}{\partial t} p + \boldsymbol{v}_g \nabla p \right] \quad (5)$$

- Solid phase:

$$\frac{\partial}{\partial t}(\varepsilon_s \rho_s h_s) + \nabla \cdot (\varepsilon_s \rho_s h_s \boldsymbol{v}_s) = -\nabla \cdot \varepsilon_s \cdot \boldsymbol{q}_s + \alpha(T_g - T_s) + \tau_s \cdot \nabla \cdot \boldsymbol{v}_s + \varepsilon_s \left[\frac{\partial}{\partial t} p + \boldsymbol{v}_s \nabla p \right] \quad (6)$$

with

$$h_i = \int_{T_{ref}}^{T} c_{p,i} \, \mathrm{d}T_i \quad \text{and} \quad \boldsymbol{q}_i = -\kappa_i \nabla T_i \quad (7)$$

2.4. Granular temperature

A balance of the solids fluctuating energy can be written as follows (see, e.g., Boemer et al. [5]):

$$\frac{3}{2}\left[\frac{\partial}{\partial t}(\varepsilon_s \rho_s \Theta_s) + \nabla \cdot (\varepsilon_s \rho_s \Theta_s) \boldsymbol{v}_s \right] = \left(-p_s^* \boldsymbol{I} + \tau_s \right) : \nabla \boldsymbol{v}_s + \nabla \cdot \left(k_\Theta^* \nabla \Theta_s \right) - \gamma_\Theta^* + \Phi_\Theta^* \quad (8)$$

The left-hand side of equation (8) is the net change of fluctuating energy. It is equal to the sum of generation of fluctuating energy $(-p_s^* \boldsymbol{I} + \tau_s) : \nabla \boldsymbol{v}_s$, the diffusion of fluctuating energy $\nabla \cdot (k_\Theta^* \nabla \Theta_s)$, the dissipation γ_Θ^* and the exchange of fluctuating energy between gas and solid phase Φ_Θ^*. A detailed discussion can be found in Boemer et al. [5].

The calculations presented in this paper use a zero flux of the granular temperature at walls.

2.5. Solid phase thermal properties

2.5.1. Interphase heat exchange

The coupling of the two energy balances occurs due to the convective heat exchange between the two phases. Within the energy equations α represents the volumetric interphase heat transfer coefficient which is the product of the specific interfacial exchange area and the fluid–particle heat transfer coefficient α_{gs}. Based on geometric considerations the following conversion can be performed:

$$\alpha = \frac{6(1 - \varepsilon_g)}{d_s} \alpha_{gs} \quad (9)$$

There are many approaches in literature which are modifications of the heat exchange model for a single sphere and a surrounding fluid (e.g., Gnielinski [10]). In fact, there are two different groups of publications on the convective heat transfer between the phases (Riquarts [11]). The first group postulates that the Nusselt number approaches a finite value as the Reynolds number vanishes, whereas the second group assumes that the limiting Nusselt number tends to zero. Schlünder [12] and Martin [13] attribute this anomalous physical behaviour to the nonuniform distribution of flow in aerated beds.

In this paper the expression from Gunn [14] has been used. This correlation is valid for a wide range of particle volume fractions, so that its application on the simulation of bubbling fluidized beds is reasonable, as the particle volume fractions range between 0 and 60 %:

$$Nu = \frac{\alpha_{gs} d_s}{\kappa_g} = \left(7 - 10\varepsilon_g + 5\varepsilon_g^2\right)\left(1 + 0.7 Re^{0.2} Pr^{1/3}\right) + \left(1.33 - 2.4\varepsilon_g + 1.2\varepsilon_g^2\right) Re^{0.7} Pr^{1/3} \quad (10)$$

2.5.2. Thermal conductivity of the solid phase

Standard approach. The thermal conductivity of the particle material differs from that of the particulate phase depending on the contacts of the particles in the fluidized beds. Based on the arrangement in a sphere packing Zehner and Schlünder [15] calculate the thermal conductivity of a bulk as a function of the thermal properties of the gas and particle material and the void fraction within the bulk. For a mathematical description within the Eulerian equations it is necessary to separate the overall bulk thermal conductivity into the thermal conductivity of the gas phase and the solid phase, respectively. This has been performed by Gidaspow and Syamlal [16] and Kuipers et al. [4]. Their expressions are:

$$\kappa_s^* = \varepsilon_p \kappa_s = \sqrt{1 - \varepsilon_g}\left[\omega \kappa_{pm} + (1 - \omega)\kappa_{cyl}\right] \quad (11)$$

$$\kappa_g^* = \varepsilon_g \kappa_g = \left(1 - \sqrt{1 - \varepsilon_g}\right)\kappa_{gas} \quad (12)$$

where the effective thermal conductivity of a cylinder κ_{cyl} is given by equation (13). This cylinder consists of one particle and the fluid phase:

$$\kappa_{cyl} = \frac{2\kappa_{gas}}{1 - B\kappa_{gas}/\kappa_{pm}}\left[\frac{(1 - \kappa_{gas}/\kappa_{pm})B}{(1 - \kappa_{gas}/\kappa_{pm}B)^2} \ln\frac{\kappa_{pm}}{B\kappa_{gas}} - \frac{B+1}{2} - \frac{B-1}{1 - B\kappa_{gas}/\kappa_{pm}}\right] \quad (13)$$

The ratio of the particle contact area to the total particle surface area ω and the factor of deformation B are given by the following expressions:

$$\omega = 7.26 \cdot 10^{-3} \quad (14)$$

$$B = 1.25\left(\frac{1 - \varepsilon_g}{\varepsilon_g}\right)^{10/9} \quad (15)$$

Kinetic approach. For a numerical simulation based on the kinetic theory of granular flows there is another promising approach to describe the thermal conductivity of a particulate phase. In the kinetic theory of gases the thermal conductivity can be understood as the exchange of kinetic energy due to collisions of the molecules. With an increase of the thermodynamic temperature the molecular fluctuations and collisions increase as well, which result in an enhanced thermal conductivity.

On the macroscopic scale of the particles, Hunt [17] introduces a model to describe the effective thermal conductivity as a function of the granular temperature, i.e. a function of the kinetic energy of the random particle fluctuations. With the help of the Maxwellian velocity distribution function the particle fluctuating velocity can be specified. This leads to the distance that a particle is travelling before colliding with another particle. In fact, this distance is a mean free path similar to that known from the kinetic theory of gases. Hunt [17] assumes that the internal energy of the particles is transfered by a so-called kinetic or streaming mechanism. Actually, this definiton only accounts for the random fluctuating particle velocity and can, therefore, not be compared with the convective transport of internal energy of the solid phase as described by the Eulerian formulation of the energy balances. Hsiau and Hunt [18] and Hunt [17] neglect collisional interactions in their definition for a thermal conductivity of the solid phase and propose a correlation for the thermal conductivity as a function of the granular temperature Θ:

$$\kappa_s^* = \varepsilon_s \kappa_s = \varepsilon_s \rho_s c_{p,s} d_s \pi^{3/2} \frac{\sqrt{\Theta}}{32 g_0} \quad (16)$$

with

$$g_0 = \frac{16 - 7\varepsilon_s}{16(1 - \varepsilon_s)^2} \quad (17)$$

Equation (17) can be identified as radial distribution function, that is used to describe the probability of interparticle collisions.

Natarajan and Hunt [19] consider an additional collisional term which has been introduced by Gelperin and Einstein [2]. From their point of view the kinetic mode is dominant at high gaseous volume fractions, whereas the collisional mode dominates at lower fractions. This model has not been implemented in the computer code so far.

Figure 1 shows the result of the effective solid phase thermal conductivity as a function of the void fraction ε_g. It is obvious that the thermal conductivity of the solid phase, predicted by Gidaspow and Syamlal [16] and Kuipers et al. [4], decreases for an increasing void fraction, since the number of particle contacts reduces. The kinetic approach shows a similar behaviour, but it considers the influence of the granular temperature. Because of the turbulent character of the random particle fluctuations, the granular temperature enhances in areas of large velocity gradients and low solid volume fractions.

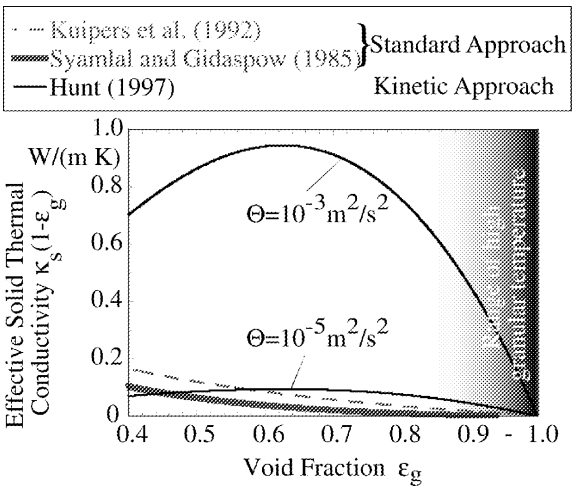

Figure 1. Effective solid phase thermal conductivity (kinetic approach versus standard approach).

Obviously, the effective thermal conductivity depends strongly on the granular temperature.

3. HEAT TRANSFER CALCULATIONS

3.1. Single bubble rising in a fluidized bed

As a first test case, the fluid dynamics and the heat transfer in a two-dimensional lab-scaled fluidized bed (height: 0.6 m, width: 0.185 m, height of the bulk: 0.25 m, particles: $d_s = 500$ µm, $\rho_s = 2\,660$ kg·m^{-3}) have been calculated. Bubbles are generated periodically at a small nozzle ($u = 5$ m·s^{-1}, $d = 5.4$ mm) placed in the middle of the distributor plate, whereas the remaining cross section is fixed in a state of minimum fluidization ($u = 0.25$ m·s^{-1}). A more detailed description is given in [6]. Due to the high computational effort, only a short period of time can be calculated during which a single bubble arises, hits the heat transfer tube ($d_{\text{Tube}} = 40$ mm) and finally bursts in the freeboard. This sequence takes about half a second in real-time. Since any additional particle class needs a further set of conservation equations, which increases the computational time, only a single particle class has been investigated. To reduce the number of grid points the calculations have been performed with a symmetry plane placed in the middle of the computational domain.

Boundary conditions and computational conditions. Figure 2 shows the boundary conditions for the numerical calculation. In contrast to a discrete element method (DEM) which calculates the movement of each particle (Rong et al. [20]), the Eulerian approach treats the particles as a continuous phase similar to the gas phase. This makes it impossible to balance the forces acting on a single particle and to decide whether it is sliding along the tube wall or if the tangential forces cause particle rotation as it is done by [20]. Due to the wall friction a no-slip velocity boundary condition for both phases has been applied. The fluctuating particle

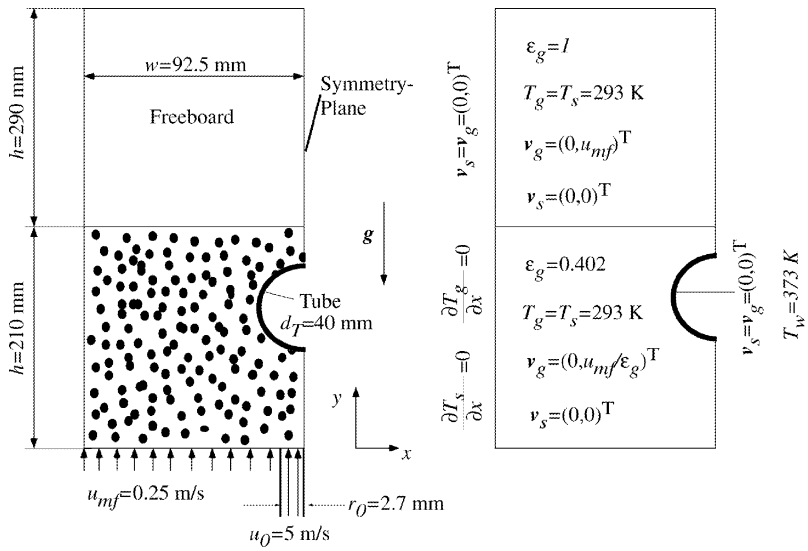

Figure 2. Sketch of the numerical set-up.

motion is described by the granular temperature. So far a zero flux of the granular temperature at all walls has been assumed. For a further numerical investigation the implementation of a new particle treatment (i.e. partial slip) introduced by Johnson and Jackson [21] will be carried out. Their approach also indicates that the sum of the flux of granular temperature and the generation of granular temperature due to local acceleration of particles is balanced by energy dissipation as a result of inelastic particle–wall collisions.

A typical time step for the numerical simulation is $2{\cdot}10^{-5}$ s. A total number of 5 500 computational cells has been used to generate a structured grid. Normal to the tube wall the smallest grid size is about 0.005 mm and increases with distance from the wall. This is sufficient to obtain a grid-independent solution.

3.1.1. Flow characteristics

Figure 3 shows a sequence of different states of particle distributions within the fluidized bed.

After 0.1 s the first bubble has just separated and starts rising through the fluidized bed. Though the bubble has not reached the heat-transfer-tube yet, the solid volume fraction is already decreasing at the bottom of the cylinder. Due to the local acceleration of the air at the lower part of the tube, a layer is observed. The air velocity exceeds the minimum fluidization velocity which leads to the formation of bubbles. Several experimental investigations (Rong et al. [20], Ozawa et al. [22]) document this phenomenon, as can be seen in *figure 4*, that has been taken from video recordings in our lab-scaled fluidized bed.

After the air bearing is large enough, small bubbles separate from the upper section of the tube.

At $t = 0.25$ s the rising bubble hits the tube. Because the velocity of this bubble is larger than the velocity of the smaller bubbles, stalling at the tube, they grow together as indicated in *figure 3* at $t = 0.3$ s. This causes a flow channel which is preferred by the rising bubble, so that a tearing apart of the bubble can be observed ($t = 0.35$ s).

The computer-simulated solid volume fractions show that the tube is always surrounded by a number of particles and the bubbles do not encase the tube completely. After the bubble has been splitted at the tube, the smaller bubbles do not coagulate any more. This can be seen at the video as well. Reminding the packet theory, this flow characteristic will influence the local tube-to-bed heat transfer due to the particle renewal. In the following section 3.1.2 this effect will be discussed in detail.

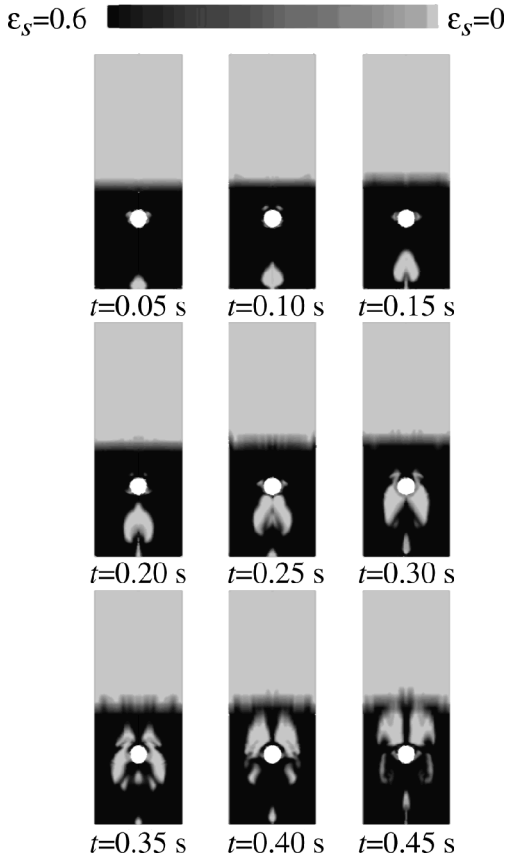

Figure 3. Bubble eruption.

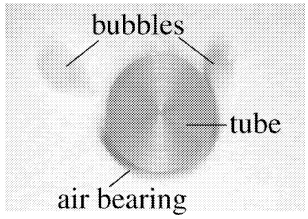

Figure 4. Particle distribution at the tube.

3.1.2. Heat transfer — comparison of physical models

Boundary conditions for the heat transfer calculations are defined as follows. The surface temperature of the tube is at 373 K, whereas the bulk has an initial temperature of 293 K and the outer walls are adiabatic. In order to obtain heat transfer coefficient from the temperature gradient at the wall, the near-wall region has to be properly resolved, since no wall functions for such dense particle flows as in fluidized beds are available. Local, instanta-

neous heat transfer coefficients can be calculated for each phase separately as given with the following equations.

- Gas phase heat transfer coefficient:

$$\alpha_{\mathrm{T,g}} = \left| \frac{\kappa_{\mathrm{g}} \partial T_{\mathrm{g}} / \partial r|_{\mathrm{W}}}{T_{\mathrm{W}} - T_{\mathrm{Bulk}}} \right| \tag{18}$$

- Solid phase heat transfer coefficient:

$$\alpha_{\mathrm{T,s}} = \left| \frac{\kappa_{\mathrm{s}} \partial T_{\mathrm{s}} / \partial r|_{\mathrm{W}}}{T_{\mathrm{W}} - T_{\mathrm{Bulk}}} \right| \tag{19}$$

Since the total heat flux is the sum of the individual fluxes $\dot{Q}_{\mathrm{T,s}}$ and $\dot{Q}_{\mathrm{T,g}}$, the overall heat transfer coefficient α_{T} can be written as the sum of $\alpha_{\mathrm{T,g}}$ and $\alpha_{\mathrm{T,s}}$.

Penetration theory. The physical boundary conditions used for the numerical simulations can hardly be realized in an experimental set-up. In the calculations the tube surface temperature is suddenly changed after an initial isothermal phase, whereas the bulk temperature is still homogeneous. This cannot be achieved by the experiments, since there always is a heating-up of the tube. Therefore, the numerical results will also be compared with an analytical approach that describes the behaviour of two semi-infinite bodies getting in contact. Kuipers et al. [4] suggested this so-called penetration theory to compare the calculated heat transfer coefficients. According to Kuipers et al. [4] the penetration theory can be applied with the following mixture properties:

$$\alpha_{\mathrm{T,pen}} = \sqrt{\frac{\kappa_{\mathrm{m}} (\rho c_p)_{\mathrm{m}}}{\pi t}} \tag{20}$$

with

$$\kappa_{\mathrm{m}} = \varepsilon_{\mathrm{g}} \kappa_{\mathrm{g}} + (1 - \varepsilon_{\mathrm{g}}) \kappa_{\mathrm{s}} \tag{21}$$

and

$$(\rho c_p)_{\mathrm{m}} = \varepsilon_{\mathrm{g}} \rho_{\mathrm{g}} c_{p,\mathrm{g}} + (1 - \varepsilon_{\mathrm{g}}) \rho_{\mathrm{s}} c_{p,\mathrm{s}} \tag{22}$$

Overall heat transfer coefficient. *Figure 5* shows the predicted instantaneous, locally averaged heat transfer coefficients, solid volume fractions and granular temperatures for the two physical models presented in section 2.5.2. Both models indicate that the solid volume fraction distribution (see *figure 5(b)*) and heat transfer at the tube are correlated. Indeed, the particles adjacent to the tube play the major role when estimating the heat transfer coefficients. In the kinetic approach the granular temperature influences the thermal transport, so *figure 5(c)* shows the local-averaged granular temperature as a function of time. Generally speaking, large values of the

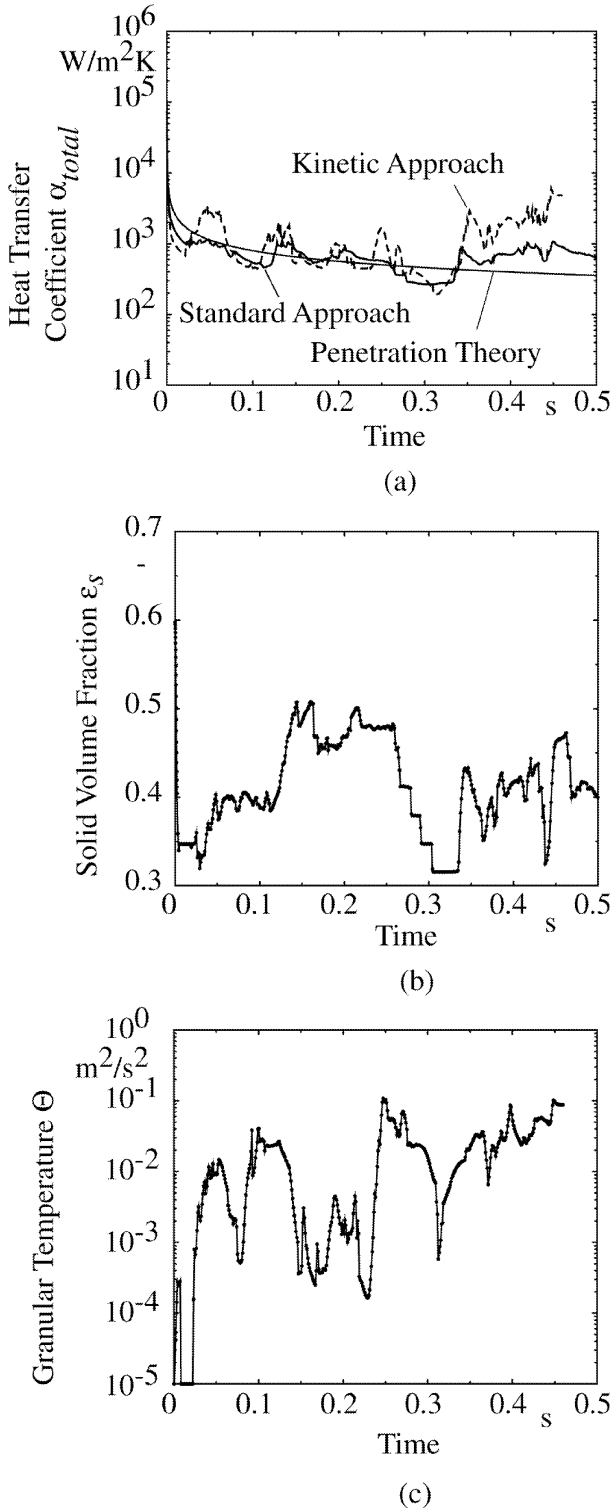

Figure 5. Instantaneous locally averaged values of heat transfer coefficient (a), solid volume fraction (b), and granular temperature (c).

granular temperature occur in areas of low solid volume fractions with low number of inter-particle collisions and large velocity gradients, which mean enhanced production of fluctuating energy. *Figures 5(a)–(c)* show average values at the circumference of the tube. This does not allow us to investigate the macroscopic mechanism of heat transfer, but gives an impression on the correlation between heat transfer and fluid dynamic. At the beginning ($t = 0$ s) the numerical simulations as well as the penetration theory predict infinite heat transfer coefficients, since the boundary condition at the tube surface is changed suddenly. The penetration theory is valid if conduction is the only transport mechanism, but since the convective part plays an important role in bubbling fluidized beds, the heat transfer coefficient is underestimated by the penetration theory. This effect is documented in *figure 5(a)*, which shows the influence of the rising bubble hitting the tube. Furthermore, if there is an air-bearing at the tube, the heat transfer decreases. Both, kinetic approach and standard approach, predict nearly the same heat transfer coefficients at the beginning of the calculation. The heat transfer rate slightly decreases with increasing time. Obviously, the relative maxima are due to the effect of small bubbles, which periodically detach from the tube and lead to a renewal of particles. At $t = 0.3$ s, when the large bubble starts getting in contact with the tube, there is a discrepancy between the two approaches, since the kinetic approach calculates heat transfer coefficients, which are larger than the values predicted from the standard approach by a factor of two. As can be seen from *figure 5(c)* the granular temperature starts increasing at $t = 0.32$ s, which means there is an increase in the fluctuating energy of the particles. This increase seems to be reasonable since the arriving bubble decreases the solid volume fraction and accelerates the particles. According to the kinetic approach the enhanced particle motion causes an increase in the effective thermal conductivity, which finally means higher heat transfer.

Local heat transfer coefficients. In order to resolve the detailed mechanisms at the tube (e.g., small bubbles detaching periodically) it is necessary to determine the local particle distributions and heat transfer values. Therefore, *figure 6* shows the heat transfer coefficient, the solid volume fraction and the granular temperature at five different positions, namely, 4, 42, 90, 137, 175°, starting anticlockwise at the top of the tube. In the near top position (i.e. $\gamma = 4°$) the numerical simulations first fit quite well the analytical solution of the penetration theory, but with increasing time both approaches differ. This can be explained with a gradual moving of particles along the tube due to an eddy which can be observed at this position, but so far there is no sudden change in the solid volume fraction. As a consequence, the analytical solution underdetermines the heat transfer rate since it neglects convection. The peak in the heat transfer characteristic at $t = 0.44$ s is caused by the bubble, which carries away particles at the tube (documented in the time-dependent solid volume fraction). Finally, this effect leads to an enhanced granular temperature that influences the effective thermal conductivity in the kinetic approach. At $\gamma = 42°$ there is only very few particle movement, so the assumptions of the penetration theory are fulfilled. Consequently, the analytical solution and the numerical calculations agree quite well. Obviously, the very small decrease in the solid volume fraction at 0.04 s, respectively 0.43 s, leads to a decrease of the total heat transfer coefficient and an enhanced granular temperature. Summarising, these two upper positions are characterised by high solid volume fractions adjacent to the tube and only little influence of bubbles on the total heat transfer.

As mentioned in section 3.1.1, small bubbles periodically detach in the lower part of the tube. This is due to the local gas acceleration, which consequently forces the excess air to generate bubbles. According to the packet theory, this flow pattern plays the major role in the heat transfer mechanism of fluidized beds. The influence of the gas–solid flow on the heat transfer is shown in *figure 6*. As a result of the turbulent particle movement, which is indicated by the high values for the granular temperature, the penetration theory is not valid any more. There is a permanent replacement of particles at the tube. Each time a new packet of "fresh" particles gets in contact with the tube surface, there is a peak in the heat transfer coefficient. Only for this short period of time, when this packet is heated up by thermal conduction, the analytical solution can be applied, starting with $t = 0$ s at the point of particle–wall contact, which predicts, mathematically speaking, infinite heat transfer coefficients decreasing again with increasing time. This phenomenon has already been investigated experimentally by Mickley et al. [23]. *Figure 7* shows their measured instantaneous heat transfer coefficients over a small time interval. Our simulations show a similar heat transfer behaviour. Fluctuating heat transfer coefficients can be observed, though the solid volume fractions, e.g., at $\gamma = 90°$ seem to be nearly constant. However, *figure 6* just displays the properties of the computational fluid-cell next to the wall at a distance of 0.005 mm and not directly at the wall. At this position ($\gamma = 90°$) a permanent particle layer is existing that damps the heat transfer. Adjacent to this position, particle renewal occurs as indicated by *figure 8*, which shows the solid volume fraction at a distance of

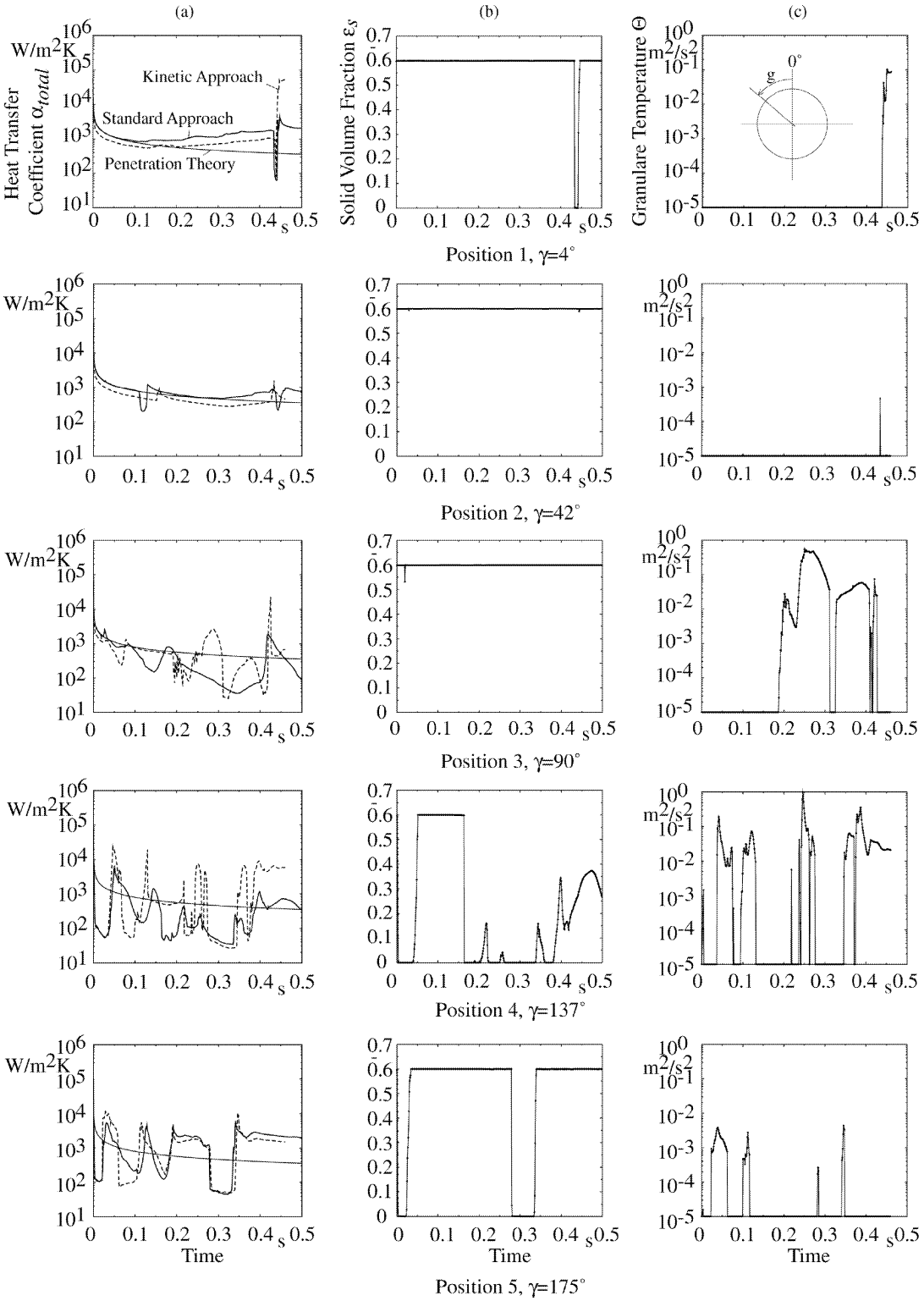

Figure 6. Numerically calculated heat transfer coefficients (a), solid volume fractions (b), and granular temperatures (c) at the tube at five positions.

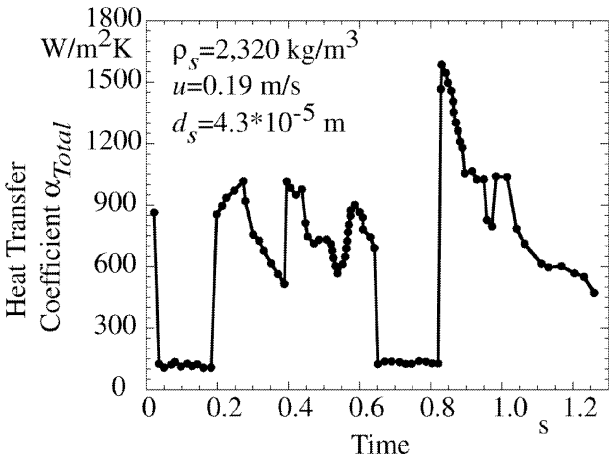

Figure 7. Measured instantaneous heat transfer coefficients (Mickley et al. [23]).

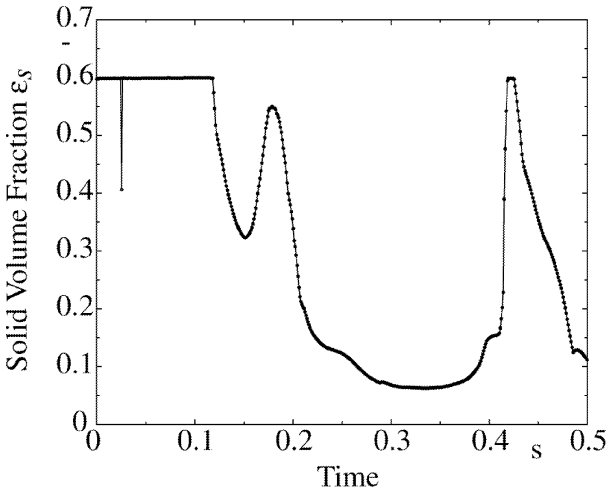

Figure 8. Solid volume fraction at $\gamma = 90°$, three cells (i.e. 0.06 mm) away from the tube surface.

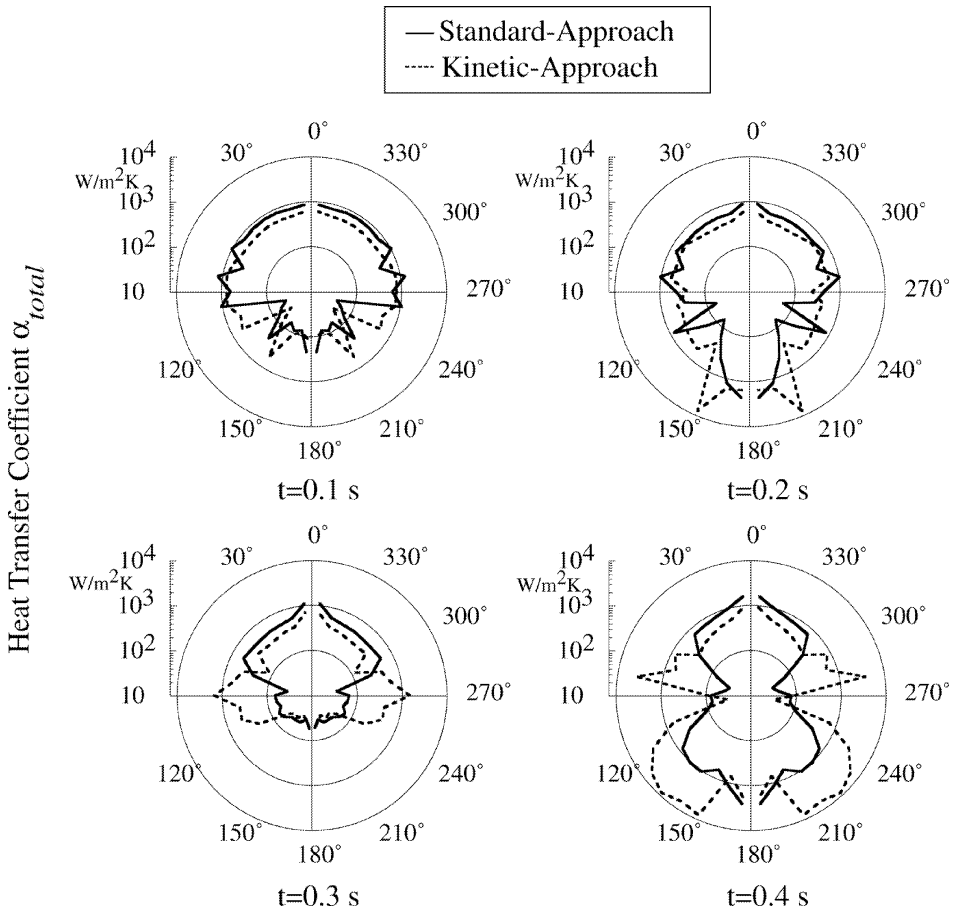

Figure 9. Local, instantaneous heat transfer coefficients.

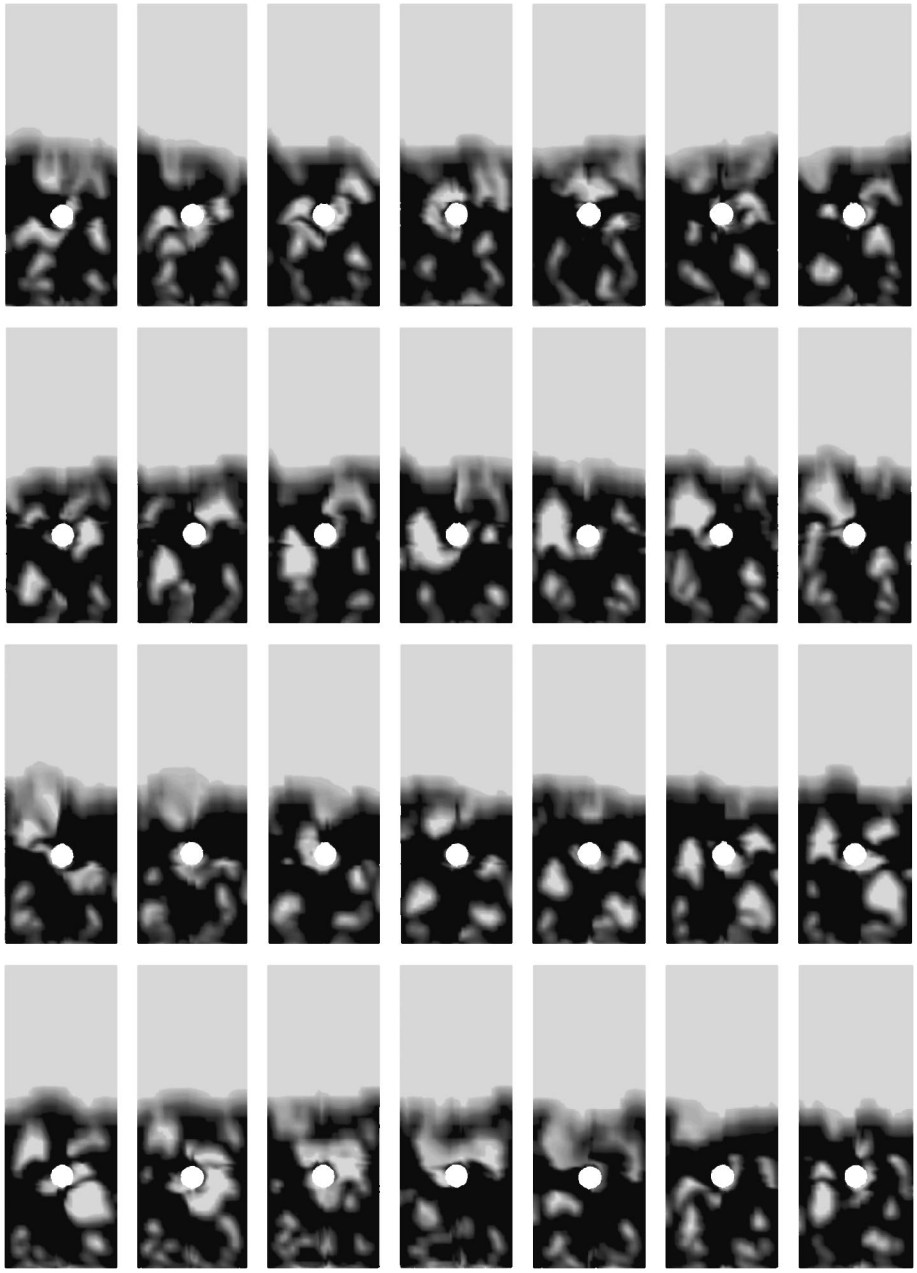

Figure 10. Spontaneous bubble formation.

about 0.06 mm away from the tube. The heat transfer coefficients can be correlated with the particle distribution adjacent to the particle layer. To find out the so-called contact time, one has to measure the temporally distance between two peaks.

The slight differences of both approaches can be explained with the dynamic behaviour of the kinetic approach, which takes into account the granular temperature as an important parameter, whereas this turbulent particle dynamic is not considered in the standard approach.

Figure 9 shows the local heat transfer coefficients at the circumference of the tube for four different times (i.e. 0.1, 0.2, 0.3 and 0.4 s). This chart gives an impres-

sion of the influence of the big bubble arriving at the tube at $t = 0.3$ s on the heat transfer. There is a decrease of the local heat transfer coefficient in the lower part of the tube, whereas the upper region is still characterised by high heat transfer coefficients. When the bubble has passed this section, the two different approaches predict an increase of the heat transfer as new particles, moving with the wake of the bubble, get in contact and improve the heat transfer characteristic. Generally speaking, the kinetic approach estimates larger values than the standard approach, which can again be explained with an increase in the granular temperature.

3.2. Spontaneous bubble formation

Whereas the calculations discussed in section 3.1 investigate the influence of a single bubble on the heat transfer in fluidized beds, this section analyses the heat transfer phenomena in spontaneously bubbling fluidized beds. In fact, this boundary condition is of much more technical interest.

3.2.1. Flow characteristics

To realize a spontaneously bubbling fluidized bed the inflow boundary conditions were changed. The air velocity at the distributor was set to a uniform value of $0.5\,\mathrm{m\cdot s^{-1}}$ and the jet was removed. As a consequence, the excess air forms bubbles spontaneously. *Figure 10* gives an impression of the predicted solid volume fractions distribution at different times. The time delay between two images is 0.05 s, so that a total sequence of 1.4 s is shown. The boundary conditions used for this calculation are the same as listed in *figure 2*. In contrast to the single bubble investigations the application of a symmetry plane is not reasonable, so that the full domain has been calculated.

3.2.2. Heat transfer investigations

Figures 11(a) and *(b)* show the calculated locally averaged heat transfer coefficients as well as the solid volume fractions at the tube as a function of time. Obviously, there is a correlation between overall heat transfer coefficient and local-averaged solid volume fraction. The fluctuating solid volume fractions are a result of the periodically emerging gas pockets as described in section 3.1. With decreasing solid volume fractions (e.g., gas pockets or gas bubbles) the overall heat transfer coefficient decreases as well. All calculations use the so-called standard approach.

To investigate the transport phenomena in detail, local values for the heat transfer coefficients and the solid volume fractions are shown at the positions 4°, 80° and 170°, in *figure 12*. In an own experimental rig thermocouples, placed in the heat transfer tube, are used to evaluate experimental heat transfer coefficients. This experimental rig is a modification of the set-up used by Röttger [24]. In contrast to the numerical set-up a three-dimensional rig has been used, having the same height and width as the computational domain shown in *figure 2*. The depth of this lab-scaled fluidized bed is 280 mm. A tube surface temperature of 373 K can be performed by a cartridge heater placed inside the tube. One of the thermocouples is fixed on the tube surface, whereas the second sensor is mounted at a depth of 7 mm inside the tube. To measure the heat transfer at different positions of the cir-

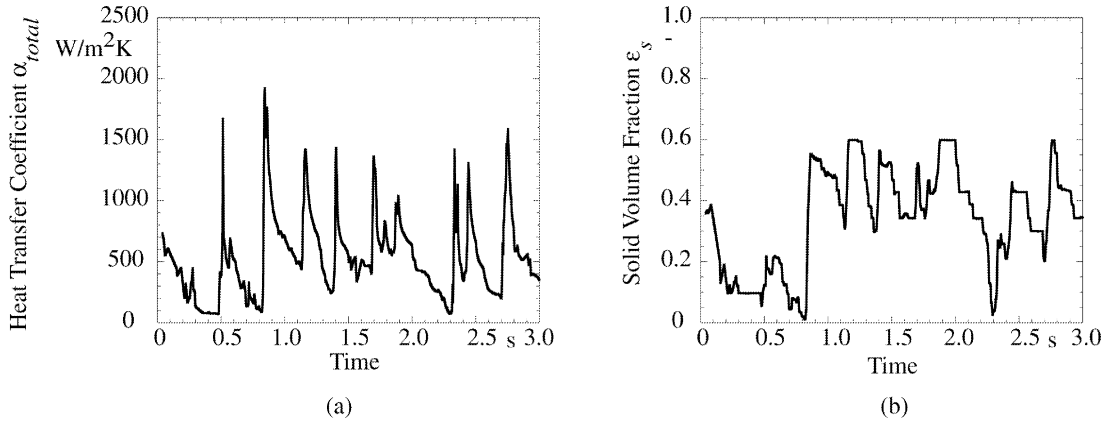

Figure 11. Locally averaged heat transfer coefficients (a) and local averaged solid volume fractions (b).

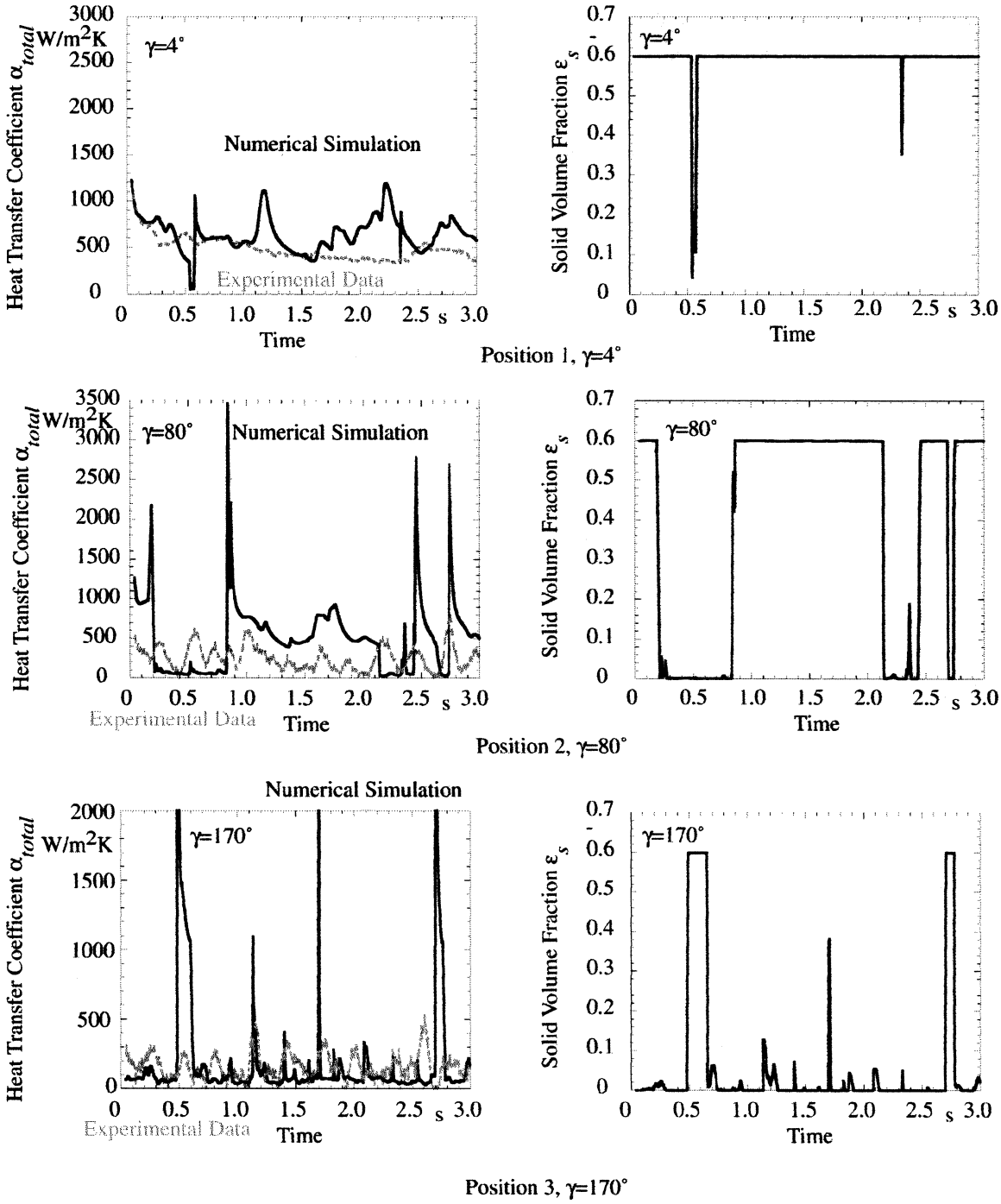

Figure 12. Comparison between numerical simulations and experimental data at different positions.

cumference, the tube can be rotated. For the evaluation of the heat transfer coefficients the one-dimensional, unsteady Fourier equation is being solved. At first, the heat transfer coefficient at the surface is an initial guess. Together with the second boundary condition (i.e. the temperature inside the tube), a temperature distribution can

be calculated. If there is a discrepancy between calculated and measured surface temperature, the heat transfer coefficient needs adjustment as long as both agree with a certain tolerance.

At the top position of the tube ($\gamma = 4°$) with low particle replacement (see *figure 12*), experimental data and numerical simulation agree well. In areas of an intensive particle replacement and bubble-to-tube contact (e.g., $\gamma = 80°$, position 2 and $\gamma = 170°$, position 3 in *figure 12*), the calculated values are much greater than those measured. Unfortunately, the actual experimental set-up is not able to resolve the instantaneous heat transfer coefficients, since their response time of 50 ms is not short enough. A fast infrared camera will solve this problem in the near future. The large increase of the instantaneous heat transfer coefficient has also been observed by Mickley et al. [23] as documented in *figure 7*.

4. CONCLUSIONS

The Eulerian approach has been used to calculate the fluid dynamics and the heat transfer in a particle–gas fluidized bed. For the mathematical description of the solid phase thermal conductivity two different models have been used. The first one is a standard approach in which the effective thermal conductivity is calculated from an idealized arrangement of the particles in the bed. In the second approach the kinetic theory of granular medias is applied to estimate the transport coefficients. The numerical simulation starts with a sudden change in the surface temperature, which leads to time-dependent heat transfer coefficients as described by the penetration theory, most experiments just show a temporal snapshot. The particle renewal at the wall leads to instantaneous high heat transfer coefficients. This phenomenon has been predicted by the calculations in agreement with experimental investigations carried out by Mickley et al. [23].

Our numerical investigations have shown that in the stagnant cap in the upper part of the tube the particle motion is very low, so that the time-dependent solution of the penetration theory is valid. At the beginning of the simulation rather high heat transfer coefficients occur at this part of the tube. With increasing time the heat transfer coefficient decreases in this area and is dominated by particle motion around the tube. The influence of the solid volume fraction (e.g., bubble formation at the tube) can be observed during the simulation. So far heat transfer coefficients and solid volume fractions were not measured simultaneously, but the fluctuating behaviour of the heat transfer coefficients in the experiments indicates a fluctuating distribution of the particles. Further investigations will be carried out with a fast infrared camera, to examine this complex correlation.

Acknowledgements

The extension of the FLUENT code for the Eulerian multiphase option is being performed in co-operation between the Lehrstuhl für Wärmeübertragung und Klimatechnik der RWTH Aachen, Germany, and Fluent Europe Ltd., Sheffield, UK. The first phase has been supported by the European Commission under contract JOU2-CT94-0452, the actual phase by the Deutsche Forschungsgemeinschaft (DFG).

REFERENCES

[1] Mickley H.S., Fairbanks D.F., Mechanism of heat transfer to fludized beds, AIChE J. 1 (3) (1955) 374–384.

[2] Gelperin N.I., Einstein V.G., Heat transfer in fluidized beds, in: Davidson J.F., Harrison D. (Eds.), Fluidization, Academic Press, London, 1971.

[3] Sundaresan S.R., Clark N.N., Local heat transfer coefficients on the circumference of a tube in a gas fluidized bed, Int. J. Multiphase Flow 21 (6) (1995) 1003–1024.

[4] Kuipers J.A.M., Prins W., van Swaaij W.P.M., Calculation of wall-to-bed heat-transfer-coefficients in gas-fluidized beds, AIChE J. 38 (1992) 1079–1091.

[5] Boemer A., Qi H., Renz U., Eulerian simulation of bubble formation at a jet in a two-dimensional fluidized beds, Int. J. Multiphase Flow 23 (5) (1997) 927–944.

[6] Schmidt A., Renz U., Eulerian computation of heat transfer in fluidized beds, Chem. Engrg. Sci. 54 (1999) 5515–5522.

[7] Savage S.B., Jeffrey D.J., Stress tensor in granular at high shear rates, J. Fluid Mech. 110 (1981) 255–272.

[8] Lun C.K.K., Savage F.B., Jeffrey D.J., Chepurnity N., Kinetic theories for granular flow: Inelastic particles in Couette flow and slightly inelastic particles in general flowfield, J. Fluid Mech. 140 (1984) 223–256.

[9] Syamlal M., Rogers W., O'Brien T.J., MFIX Documentation, Theory Guide, Technical Note DOE/METC-94/1004, 1993.

[10] Gnielinski V., Gleichungen zur Berechnung des Wärme- und Stoffaustausches in durchströmten ruhenden Kugelschüttungen bei mittleren und großen Pecletzahlen, Verfahrenstechnik 12 (1978) 363–366.

[11] Riquarts H.P., On heat transfer between particles and fluid in aerated beds, Germ. Chem. Engrg. 3 (1980) 286–295.

[12] Schlünder E.U., On the mechanism of mass transfer in heterogeneous systems, Chem. Engrg. Sci. 32 (1977) 845–851.

[13] Martin H., Low Peclet number particle-to-fluid heat and mass transfer in packed beds, Chem. Engrg. Sci. 33 (1978) 913–919.

[14] Gunn D.J., Transfer of heat or mass to particles in fixed and fluidized beds, Int. J. Heat Mass Tran. 21 (1978) 467–476.

[15] Zehner P., Schlünder E.U., Wärmeleitfähigkeit von Schüttungen bei mäßigen Temperaturen, Chemie Ing. Techn. 42 (14) (1970) 933–941.

[16] Gidaspow D., Syamlal M., Hydrodynamics of fluidization: Prediction of wall to bed heat transfer coefficients, AIChE J. 31 (1) (1985) 127–135.

[17] Hunt M.L., Discrete element simulations for granular material flows: Effective thermal conductivity and self diffusivity, Int. J. Heat Mass Tran. 40 (13) (1997) 3059–3068.

[18] Hsiau S.S., Hunt M.L., Shear-induced particle diffusion and longitudinal velocity fluctuations in a granular-flow mixing layer, J. Fluid Mech. 251 (1993) 299–313.

[19] Natarajan V.V.R., Hunt M.L., Kinetic theory analysis of heat transfer in granular flows, Int. J. Heat Mass Tran. 41 (13) (1998) 1929–1944.

[20] Rong D., Mikami T., Horio M., Particle and bubble movements around tubes immersed in fluidized beds — a numerical study, Chem. Engrg. Sci. 54 (1999) 5737–5754.

[21] Johnson P.C., Jackson R., Frictional–collisional constitutive relations for granular materials, with application to plane shearing, J. Fluid Mech. 176 (1987) 67–93.

[22] Ozawa M., Umekawa H., Matsuda T., Local void fraction distribution and heat transfer in tube-banks immersed in a fluidized bed, in: Heat Transfer, Proceedings of the 11th IHTC, Vol. 2, August 23–28, Kyongju, Korea, 1998, pp. 75–80.

[23] Mickley H.S., Fairbanks D.F., Hawthorn R.D., The relation between the heat transfer coefficient and thermal fluctuations in fluidized-bed heat transfer, Chem. Engrg. Progr. Symp. Ser. 57 (32) (1961) 51–60.

[24] Röttger H.J., Renz U., Measurement of instantaneous local heat transfer coefficients around a tube immersed in a high temperature fluidized bed, in: Proceedings of the 10th Int. Heat Transfer Conference, Vol. 2, Brighton, UK, August 14–18, 1994, pp. 285–290.